Journal of Power Sources 196 (2011) 4821–4825

Contents lists available at ScienceDirect

Journal of Power Sources

journal homepage: www.elsevier.com/locate/jpowsour

Short communication

Synthesis and electrochemical performance of the high voltage cathode material $Li[Li_{0.2}Mn_{0.56}Ni_{0.16}Co_{0.08}]O_2$ with improved rate capability

J. Li, R. Klöpsch, M.C. Stan, S. Nowak, M. Kunze, M. Winter, S. Passerini*

Institute of Physical Chemistry, University of Muenster, Corrensstr. 28/30, 48149 Muenster, Germany

ARTICLE INFO

Article history:
Received 14 October 2010
Received in revised form
17 December 2010
Accepted 3 January 2011
Available online 14 January 2011

Keywords:
Lithium-ion battery
Cathode material
$Li[Li_{0.2}Mn_{0.56}Ni_{0.16}Co_{0.08}]O_2$
NMC
Cycling performance
Rate capability

ABSTRACT

The high voltage layered $Li[Li_{0.2}Mn_{0.56}Ni_{0.16}Co_{0.08}]O_2$ cathode material, which is a solid solution between Li_2MnO_3 and $LiMn_{0.4}Ni_{0.4}Co_{0.2}O_2$, has been synthesized by co-precipitation method followed by high temperature annealing at 900 °C. XRD and SEM characterizations proved that the as prepared powder is constituted of small and homogenous particles (100–300 nm), which are seen to enhance the material rate capability. After the initial decay, no obvious capacity fading was observed when cycling the material at different rates. Steady-state reversible capacities of 220 mAh g^{-1} at 0.2*C*, 190 mAh g^{-1} at 1*C*, 155 mAh g^{-1} at 5*C* and 110 mAh g^{-1} at 20*C* were achieved in long-term cycle tests within the voltage cutoff limits of 2.5 and 4.8 V at 20 °C.

1. Introduction

Layered transition metal oxides have been investigated extensively as cathode materials for lithium-ion batteries. There into, $LiCoO_2$ is the most important commercial material because of its very good electrochemical performance. However, on the other hand, it also suffers some drawbacks, such as high cost, toxicity, and safety problems, which inhibit its further use in hybrid and pure electric vehicles [1–3]. The identification of a cheaper, higher capacity and safer layered cathode materials has been the focusing point in the study of cathode materials in the last decade. In this regard, the solid solutions of layered Li_2MnO_3 and $LiMO_2$ (M = Mn, Co, Ni, etc.) have been shown as promising candidates for cathode materials in lithium ion batteries since they exhibit a relatively high capacity, low cost and improved safety [2,4–11]. Two members of this family, $Li[Li_{0.2}Mn_{0.6}Ni_{0.2}]O_2$, which can be indicated as $0.6Li_2MnO_3{\cdot}0.4LiMn_{0.5}Ni_{0.5}O_2$, and $Li[Li_{0.2}Mn_{0.54}Ni_{0.13}Co_{0.13}]O_2$ (also indicated as $0.6Li_2MnO_3{\cdot}0.4LiMn_{1/3}Ni_{1/3}Co_{1/3}O_2$), are widely investigated already. Usually, these materials deliver an initial capacity of about 250 mAh g^{-1} within the potential range extending from 2.0 to 4.8 V [8–12]. Between them, $Li[Li_{0.2}Mn_{0.54}Ni_{0.13}Co_{0.13}]O_2$ always shows better performance because of the presence of cobalt that significantly reduce the electrode polarization and improve the activation of the Li_2MnO_3 component, even if present in a small amount [13,14]. Nevertheless, the long-term cycling performance of this latter material is still not very satisfactory. In addition, it still contains 13 mol% of Co, which certainly represents an issue with regard to cost. Finally, most of the works on these materials report the electrochemical performance at very low current rates (such as *C*/20), which is of no help to ascertain their capability of matching with the requirement of today's lithium ion batteries.

In this work, we report on the synthesis and characterization of a novel cathode material with a substantially lower Co content. The material has a general formula of $Li[Li_{0.2}Mn_{0.56}Ni_{0.16}Co_{0.08}]O_2$, which can also be seen as the solid solution of Li_2MnO_3 and $LiMn_{0.4}Ni_{0.4}Co_{0.2}O_2$ in 6:4 molar ratio. The structure, physical properties and electrochemical performance are reported in the following, with a special attention to the rate capabilities at high current rates.

2. Experimental

$Li[Li_{0.2}Mn_{0.56}Ni_{0.16}Co_{0.08}]O_2$ was synthesized by a solid-state reaction method from lithium hydroxide hydrate ($LiOH{\cdot}H_2O$ Aldrich >98%) and manganese–nickel–cobalt hydroxide precursor [15]. This precursor was prepared by co-precipitating the aqueous solution of the three metal acetate salts (Mn, Ni, and Co; Aldrich >98%) in a stoichiometric ratio of 56:16:8, with lithium hydroxide. After extensive rinsing with distilled water, the precipitate

* Corresponding author. Tel.: +49 251 8336026; fax: +49 251 8336032.
E-mail address: stefano.passerini@uni-muenster.de (S. Passerini).

0378-7753/$ – see front matter © 2011 Elsevier B.V. All rights reserved.
doi:10.1016/j.jpowsour.2011.01.006

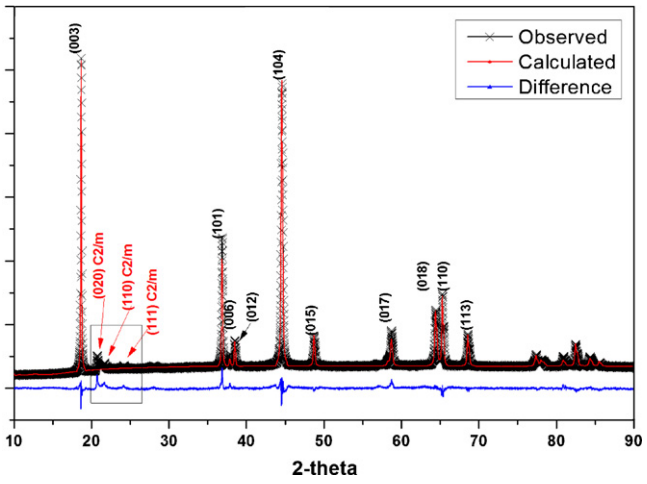

Fig. 1. Rietveld refinement results for the XRD pattern of $Li[Li_{0.2}Mn_{0.56}Ni_{0.16}Co_{0.08}]O_2$ material by GSAS.

was dried under vacuum at 120 °C overnight. The dried material was then mixed with a stoichiometric amount of $LiOH{\cdot}H_2O$ by ball milling for 5 h in the zirconia jar. After suitable grinding, the mixture was annealed in air at 480 °C for 5 h, and then, as a pellet, at 900 °C for 24 h. The final material was obtained by quenching the pellet in liquid nitrogen in order to "freeze" the layered solid-solution phase.

The composition in terms of lithium and transition metal contents in the active material was determined by the inductively coupled plasma optical emission spectrometry (ICP-OES, SPECTRO ARCOS, Ametek, Germany). The crystalline structure was characterized by X-ray diffraction (XRD) using the Cu Kα radiation on the Bruker D8 Advance (Germany) in the 2θ range from 10° to 90°. Lattice parameters were determined by Rietveld refinement with GSAS software. The particle size distribution was evaluated with the help of a high resolution Scanning Electron Microscopy (SEM, EVO® MA 10 microscope, Zeiss). The BET surface area and solid phase density were measured by using the ASAP 2020 and the AccuPyc II 1340 from Micromeritics Instrument Corporation (USA).

Electrodes were prepared by casting the slurry, with the composition of 80 wt% active material (by weight), 10 wt% Super P (TIMCAL), and 10 wt% PVDF (Kynar® FLEX 2801, Arkema Group), onto Al foil. The electrode active material mass loading was about 2 mg cm^{-2} while the thickness (after pressing at 3–4 tons cm^{-2} for 30 s) was 10 μm. With metal lithium foil as the counter and reference electrodes, the cathode electrodes were assembled into swagelok cells with the 1 M $LiPF_6$ in 1:1 EC:DMC solution as the electrolyte. Cells were cycled galvanostatically at different constant current rates (nominal capacity = 200 mAh g^{-1}, $1C$ = 200 mA g^{-1}) between 4.8 V and 2.5 V at 20 °C using Maccor series 4000 battery tester (USA). All potential reported in this work refer to the Li/Li^+ couple.

All experiments, including synthesis, were duplicated to check reproducibility.

3. Results and discussion

Fig. 1 shows the XRD pattern and the Rietveld refinement results of $Li[Li_{0.2}Mn_{0.56}Ni_{0.16}Co_{0.08}]O_2$. The values of χ^2 (4.926) and Rwp (9.9%) demonstrate a satisfactory refinement. With the exclusion of the low intensity reflections, in particular those within 20° and 25°, the crystal lattice was approximated as signed to the layered structure with space group of $R\bar{3}m$ [3], the intensity ratio of the (0 0 3) and (1 0 4) peaks (equal to 1.11), and the clear splitting of the (1 0 8) and (1 1 0) peaks suggest an ordering structure of $R\bar{3}m$ single phase.

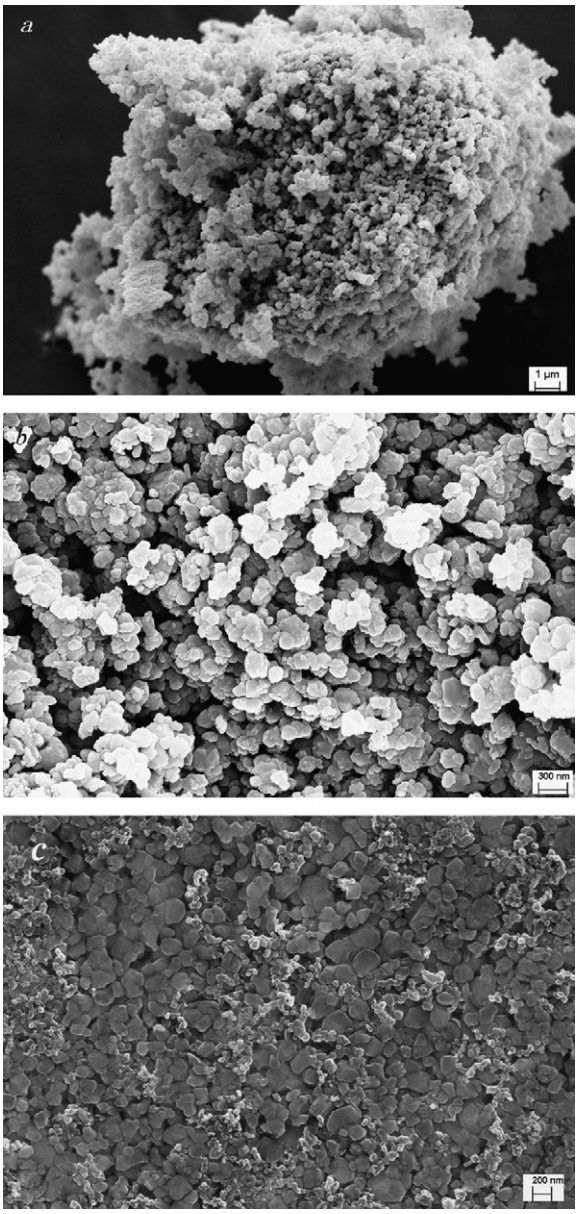

Fig. 2. SEM pictures of $Li[Li_{0.2}Mn_{0.56}Ni_{0.16}Co_{0.08}]O_2$ material at different magnifications. (a) ×5k; (b and c) ×50k.

The hexagonal lattice parameters were refined to be a = 2.8560(1) Å, c = 14.283(2) Å, and volume = 100.65(2) $Å^3$, with a c/a ratio of 4.99. The weak reflections are known to originate from the monoclinic Li_2MnO_3-like ($C2/m$) super lattice [16], which correspond to the ordering of the Li^+, Ni^{2+}, and Mn^{4+} ions in the transition metal layer [17].

The ICP-OES analysis indicated the molar ratio of Li and the transition metal ions to be Li:Mn:Ni:Co = 1.21:0.53:0.17:0.09, i.e., in good agreement with the composition of the starting reactants. The crystallite size was calculated from XRD by using the Scherrer's formula [1] for the three main reflection peaks, e.g. (0 0 3), (1 0 1) and (1 0 4). The average result is 89 nm which is smaller than that of the pure $LiMn_{0.4}Ni_{0.4}Co_{0.2}O_2$ prepared with the same annealing conditions [18].

The morphology of the $Li[Li_{0.2}Mn_{0.56}Ni_{0.16}Co_{0.08}]O_2$ particles and pressed electrode, investigated by scanning electron microscopy, is shown in Fig. 2. The SEM image in Fig. 2a shows that the powder contains aggregates of primary, round sharp particles. These primary particles, which are better observed in

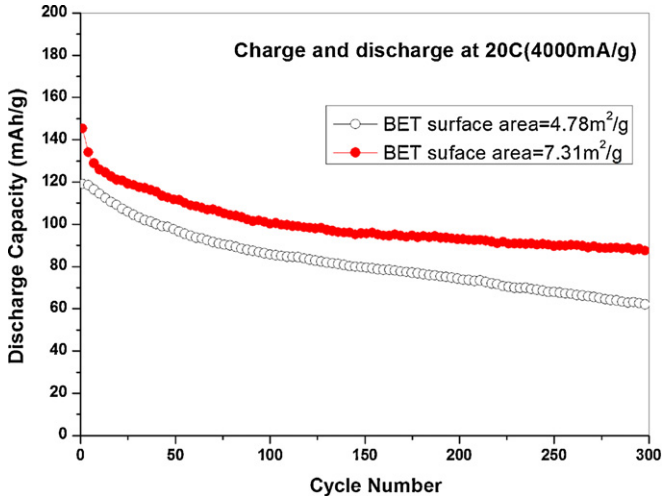

Fig. 3. Comparison of high rate (20*C*) cycling performance of $Li[Li_{0.2}Mn_{0.56}Ni_{0.16}Co_{0.08}]O_2$ electrodes with different particle sizes.

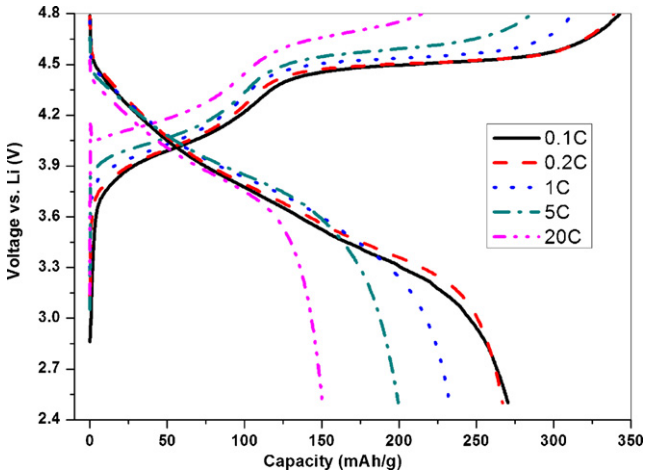

Fig. 4. First charge and discharge profiles of $Li[Li_{0.2}Mn_{0.56}Ni_{0.16}Co_{0.08}]O_2$ electrodes as cycled at different rates in the voltage range between 2.5 V and 4.8 V at 20 °C.

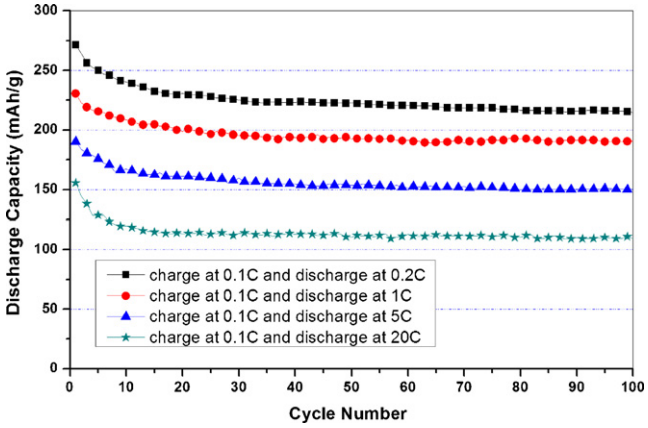

Fig. 5. Cycling performance of $Li[Li_{0.2}Mn_{0.56}Ni_{0.16}Co_{0.08}]O_2$ electrodes charged at 0.1*C* and discharged at different rates. The tests carried out in the voltage range between 2.5 V and 4.8 V at 20 °C.

Fig. 2b, are homogenous and have a small size between 100 and 300 nm. Since small particles present shorter diffusion path for Li ions, the insertion and de-insertion of the Li in this material are expected to be faster [1,19,20]. The SEM image of pressed electrode is shown in Fig. 2c. It can be seen that the electrode is composed of a very homogenous mixture of primary active material and Super P. In addition, the specific surface area for the prepared $Li[Li_{0.2}Mn_{0.56}Ni_{0.16}Co_{0.08}]O_2$ powder, as detected by BET, is 7.31 $m^2\,g^{-1}$, which is much higher than that of commercial $LiMn_{1/3}Ni_{1/3}Co_{1/3}O_2$ material (0.61 $m^2\,g^{-1}$, TODA Kogyo Europe GmbH). In addition, the average particle size calculated from the solid phase density of 4.30 g cm^{-2} and BET surface area (7.31 $m^2\,g^{-1}$), is 190 nm, which is in very good agreement with the 100–300 nm particle size detected by SEM. Such a high surface area is expected to favor the charge transfer process of lithium ions thus enhancing the electrochemical performance of this material, especially the high rate capability. This is well shown in Fig. 3 where the comparison of the rate performance for different BET surface area materials is shown. The material having a BET surface area of 4.78 $m^2\,g^{-1}$ (corresponding to 290 nm average particle size) shows a worse high rate (20*C*) performance than the small particle size material in terms of both capacity and cycling stability. In fact, the larger particle size material delivered only 119 mAh g^{-1} at the 1st cycle and 61.6 mAh g^{-1} after 300 cycles against 145.4 mAh g^{-1} and 87.2 mAh g^{-1}, respectively, delivered by the smaller particle size material. This result proved that the smaller particle will lead to better performance at high rate cycling.

Fig. 4 compares the first charge–discharge profiles of $Li[Li_{0.2}Mn_{0.56}Ni_{0.16}Co_{0.08}]O_2$ cathode at different current densities. As expected from the XRD characterization, the material exhibited two plateaus during the first charge, due to the existence of two different lithium de-insertion processes [6]. Both plateaus shifted to higher potential with the increase of current. In the first plateau, which is located at 3.8–4.4/4.5 V, all electrodes delivered almost the same capacity (about 110–120 mA g^{-1}) independent on the current used. This plateau is associated to the delithiation of the $LiMn_{0.4}Ni_{0.4}Co_{0.2}O_2$-like regions [21] that corresponds to the oxidation of $Ni^{2+} \rightarrow Ni^{4+}$ and $Co^{3+} \rightarrow Co^{4+}$. Since the rate capability of these two processes is improved by the participation of the Li ions in the transition metal layer [22], the charge delivered in the first plateau is very close to the theoretical capacity of 111.5 mAh g^{-1}. The second plateau, which is located above 4.4/4.5 V during charging, is widely accepted to originate from the loss of oxygen from the layered Li_2MnO_3 lattice [6], which might be transformed in a MnO_2-like phase. The capacity delivered in this second plateau strongly decreases as the current increases (220 mAh g^{-1} at 0.1*C* against 105 mAh g^{-1} at 20*C*) thus indicating that this process has rather slow kinetics.

The capacity delivered during the first discharge is obviously resulting from the insertion of lithium in both the $LiMn_{0.4}Ni_{0.4}Co_{0.2}O_2$-like regions and the MnO_2-like regions.

Fig. 5 compares the capacity retention of $Li[Li_{0.2}Mn_{0.56}Ni_{0.16}Co_{0.08}]O_2$ electrodes when charged at 0.1*C* and discharged at different current rates (0.2*C*, 1*C*, 5*C* and 20*C*) within the cut-off voltages of 2.5 V and 4.8 V (20 °C). The delivered capacities at the 1st, 30th, 80th and 100th cycles are also listed in Table 1. In the first discharge process, the electrodes were able to deliver capacities of 271.4 mAh g^{-1} and 230.6 mAh g^{-1} at 0.2*C* and 1*C*, respectively. Very interestingly, at 5*C* and 20*C*

Table 1
Capacity of $Li[Li_{0.2}Mn_{0.56}Ni_{0.16}Co_{0.08}]O_2$ electrodes discharged at different rates. Charge rate was always 0.1*C*.

Cycle	Discharge capacity (mAh g^{-1})			
	0.2*C*	1*C*	5*C*	20*C*
1st	271.5	230.6	195.3	155.4
30th	225.1	195.4	164.6	113.7
80th	217.4	192.8	155.9	110.4
100th	214.6	190.7	155.0	109.4

rates, the electrodes were still able to deliver 195.3 mAh g^{-1} and 155.4 mAh g^{-1}, respectively, which corresponded to 72% and 57% of the 0.2*C* delivered capacity. This comparison clearly indicates the promising high rate capability of the material. However, the discharge capacities decreased in the next several cycles independent on the current used in the test. At the 30th cycle, the capacity dropped to 225.1 mAh g^{-1} at 0.2*C* (i.e., 82.9% of the 1st cycle capacity), and 113.4 mAh g^{-1} at 20*C* (i.e., 73.1% of the 1st cycle capacity). However, after the 30th cycle the capacity fade was much less significant at all rates. It is proved that capacities as high as 217.4 mAh g^{-1} after 80 cycles at 0.2*C* rate, and 190.7 mAh g^{-1}, 155.5 mAh g^{-1} and 109.4 mAh g^{-1} after 100 cycles at 1*C*, 5*C* and 20*C*, respectively, were obtained. The comparison with the values obtained at the 30th cycle indicates that only a minor capacity loss, i.e., less than 8 mAh g^{-1}, took place. This proves that this material is a good candidate for high discharge rate electrodes even though the capacity retention in the initial 20 or 30 cycles still needs to be improved. Nevertheless, it is important to notice that the capacity delivered by our material during the 100th discharge at 1*C* rate very well compare with that of the Li–Ni–PO_4 coated $0.5Li_2MnO_3{\cdot}0.5LiMn_{1/3}Ni_{1/3}Co_{1/3}O_2$ which is reported to have the better cycle stability at high rate [23]. Unfortunately, direct comparison with long term high rate test of other materials from the same family is not possible so far till now due to the lack of literature data. In fact, most of the reports present results which are limited in both the cycle number and rate capability. To the best our knowledge, our material has shown the best cycle stability during long-term test.

Because of the above mentioned high discharge rate performance, the material was then tested at high charge current. Fig. 6 shows the delivered capacities of $Li[Li_{0.2}Mn_{0.56}Ni_{0.16}Co_{0.08}]O_2$ electrodes charged and discharged at the same current rate within the cut-off voltage of 2.5 V and 4.8 V (20 °C). The delivered capacities in the 1st, 30th, 100th, and 300th cycles are also listed in Table 2. From Fig. 6, it is seen that the electrodes achieved first cycle discharge capacities of 266.8 mAh g^{-1}, 233.6 mAh g^{-1}, 191.3 mAh g^{-1} and 145.4 mAh g^{-1} at 0.2*C*, 1*C*, 5*C* and 20*C*, respectively. These values are only slightly lower than those obtained with the charging process at 0.1*C* (Table 1), thus indicating that the charge rate

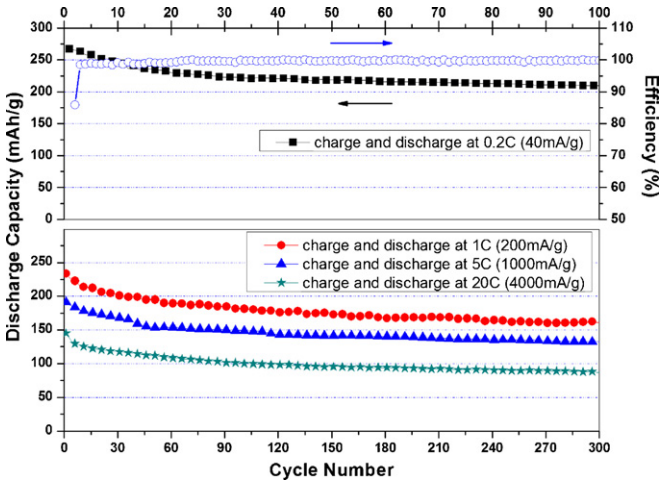

Fig. 6. Cycling performance of $Li[Li_{0.2}Mn_{0.56}Ni_{0.16}Co_{0.08}]O_2$ electrodes subjected to continuous cycling at different rates (0.2*C*, 1*C*, 5*C* and 20*C*). Charged and discharged at the same rate. The tests were carried out in the voltage range between 2.5 V and 4.8 V at 20 °C. The low rate test date (0.2*C*) is referred to the upper cycle number scale. The charge efficiency during the cycle test at 0.2*C* is also reported.

Table 2
Capacity of $Li[Li_{0.2}Mn_{0.56}Ni_{0.16}Co_{0.08}]O_2$ electrodes charged and discharged at different rates.

Cycle	Discharge capacity (mAh g^{-1})			
	0.2*C*	1*C*	5*C*	20*C*
1st	266.8	233.6	191.3	145.4
30th	223.1	201.7	168.4	118.2
100th	209.4	181.5	148.9	100.3
300th		161.0	132.5	87.2

does not strongly affect the material performance. Furthermore, the capacity delivered by the electrode charged at 20*C* was 54.5% of that delivered by the electrode tested at 0.2*C*. This latter value is practically coincident with the result of Fig. 5. After 30 cycles, the material maintained the similar capacity of 223.1 mAh g^{-1} for the

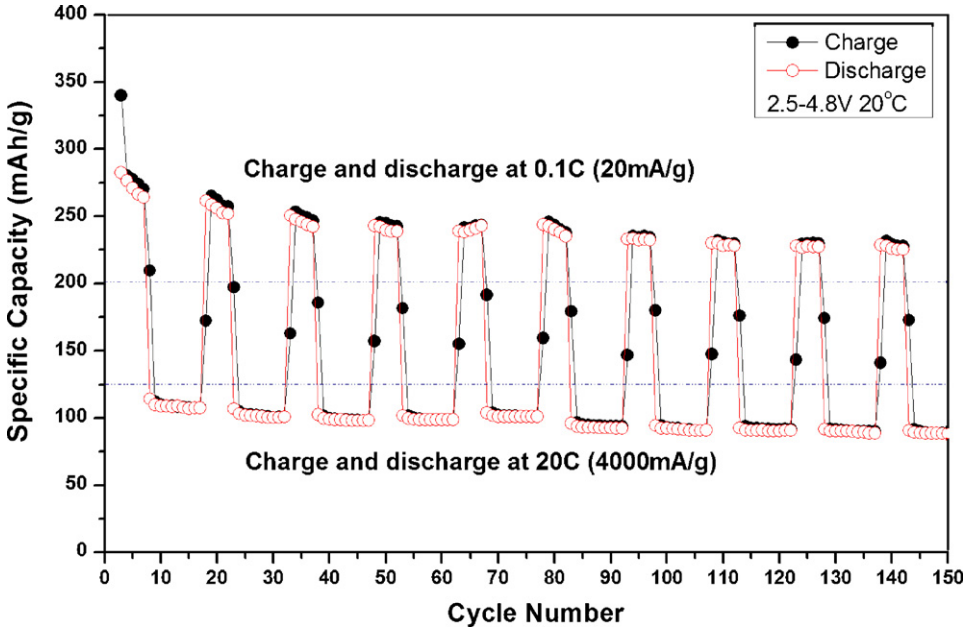

Fig. 7. Cycling performance of a $Li[Li_{0.2}Mn_{0.56}Ni_{0.16}Co_{0.08}]O_2$ electrode cycled at, alternatively, 0.1*C* and 20*C*. The test was carried out in the voltage range between 2.5 V and 4.8 V at 20 °C. The anomalous capacity behavior recorded between the 60th and the 80th cycles is due to a temperature increase (from 20 °C to 25 °C), which affected all cells under test.

low 0.2*C* rate, but got even a little more for the high C-rate like 1*C*, 5*C* and 20*C*. Then, it is expected that this material is not only useful for high rate discharging, but also for high rate charging. As already pointed out, the unsatisfying performance here is still the capacity decrease during the initial cycles independent on the current rate.

The long-term fading phenomenon after the 30th cycle, especially seen in the high rate test appeared however, to be associated with kinetics rather than degradation. Fig. 7 shows the capacity vs. cycle number behavior of a $Li[Li_{0.2}Mn_{0.56}Ni_{0.16}Co_{0.08}]O_2$ electrode subjected to consecutive set of cycles at low (0.1*C*) and high (20*C*) charge and discharge rates. This double rate test was performed by charging and discharging the electrode at 0.1*C* for 5 cycles, and then at 20*C* (both charge and discharge) for the next ten cycles. The test was performed within the voltage range between 2.5 V and 4.8 V, by repeating the steps for several times. Considering only the low rate cycles, it is seen that the electrode behaved very similarly to the one reported in Fig. 6. It delivered 263.9 mAh g^{-1} at the 5th cycle with only a small decrease (261.7 mAh g^{-1}) at the 16th cycle, i.e., after ten cycles at 20*C*. In practice, the high rate cycling did not affect much the capacity fading of the material at low rate. As a matter of fact, the electrode reached the steady-state conditions after 35 low rate cycles with a stable delivered capacity of 225 mAh g^{-1} (0.1*C*). The delivered capacity during the high rate cycling also shows the same behaviors as the electrode cycled at high rate only (see Fig. 6). However, the continuous capacity fading does not match with the stable trend detected on the same electrode at low rate. This indicates that increasing the rate from 0.1*C* to 20*C* does not lead to a degradation of this material but rather to a degradation of the composite electrode morphology, which affects only the high rate cycling. It also confirms that $Li[Li_{0.2}Mn_{0.56}Ni_{0.16}Co_{0.08}]O_2$ cathode material can be used in lithium ion batteries operating in very flexible current conditions.

4. Conclusions

The layered $Li[Li_{0.2}Mn_{0.56}Ni_{0.16}Co_{0.08}]O_2$ solid solution has been successful synthesized by co-precipitation method. The material shows the single phase layered with the super lattice structure originating from the monoclinic Li_2MnO_3. The primary particles are homogenous and small in size (100–300 nm), which was found to be very helpful to reduce the lithium diffusion time in the material.

The highlights of this material are its high delivered capacity and good rate capability. In fact, it can achieve around 270 mAh g^{-1} at 0.2*C* and 150 mAh g^{-1} at 20*C* in the first cycle, while offering steady-state reversible capacities of around 220 mAh g^{-1} at 0.2*C* and 110 mA g^{-1} at 20*C*. The material can be used not only in high current charge but also in high current discharge, and the cells still work well. Even after 300 cycles at high C-rate, like 5*C* and 20*C*. In addition, the current rate can be changed freely without any bad influence to the electrode performance. All of the results prove that the material can be used under very flexible conditions. In summary, this cathode material may meet and exceed the lithium ion batteries requirements for use in hybrid-electric vehicles and other devices requiring high energy and power. However, it still suffers the drawback of capacity fading during the initial cycling. Work is in progress to improve its cycling performance by appropriate surface modification, which will be reported in the near future.

Acknowledgement

The authors kindly acknowledge the financial support of BMBF – Competence Alliance North: Electrochemistry for Electromobility.

References

[1] X.Y. Zhang, W.J. Jiang, A. Mauger, Qilu, F. Gendron, C.M. Julien, J. Power Sources 195 (2010) 1292.
[2] J.M. Zheng, J. Li, Z.R. Zhang, X.J. Guo, Y. Yang, Solid State Ionics 179 (2008) 1794.
[3] J. Li, J.M. Zheng, Y. Yang, J. Electrochem. Soc. 154 (2007) A427.
[4] M.M. Thackeray, S.H. Kang, C.S. Johnson, J.T. Vaughey, R. Benedek, S.A. Hackney, J. Mater. Chem. 17 (2007) 12.
[5] C.S. Johnson, N.C. Li, C. Lefief, J.T. Vaughey, M.M. Thackeray, Chem. Mater. 20 (2008) 6095.
[6] J.S. Kim, C.S. Johnson, J.T. Vaughey, M.M. Thackeray, S.A. Hackney, Chem. Mater. 16 (2004) 1996.
[7] T.A. Arunkumar, E. Alvarez, A. Manthiram, J. Mater. Chem. 18 (2008) 190.
[8] J. Gao, J. Kim, A. Manthiram, Electrochem. Commun. 11 (2009) 84.
[9] J. Gao, A. Manthiram, J. Power Sources 191 (2009) 644.
[10] X.J. Guo, Y.X. Li, M. Zheng, J.M. Zheng, J. Li, Z.L. Gong, Y. Yang, J. Power Sources 184 (2008) 414.
[11] Y. Wu, A. Manthiram, Electrochem. Solid State Lett. 9 (2006) A221.
[12] Q.Y. Wang, J. Liu, A.V. Murugan, A. Manthiram, J. Mater. Chem. 19 (2009) 4965.
[13] S.H. Kang, P. Kempgens, S. Greenbaum, A.J. Kropf, K. Amine, M.M. Thackeray, J. Mater. Chem. 17 (2007) 2069.
[14] M.M. Thackeray, S.H. Kang, C.S. Johnson, J.T. Vaughey, S.A. Hackney, Electrochem. Commun. 8 (2006) 1531.
[15] J. Li, J.M. Zheng, X.J. Guo, Z.L. Gong, Y. Yang, Chem. J. Chin. Univ. 27 (2006) 1.
[16] A. Boulineau, L. Croguennec, C. Delmas, F. Weill, Solid State Ionics 180 (2010) 1652.
[17] T.A. Arinkumar, Y. Wu, A. Manthiram, Chem. Mater. 19 (2007) 3067.
[18] S.K. Martha, H. Sclar, Z.S. Framowitz, D. Kovacheva, N. Saliyski, Y. Gofer, J. Power Sources 189 (2009) 248.
[19] Q.W. Peng, Z.Y. Tang, L.Q. Zhang, X.J. Li, Mater. Res. Bull. 44 (2009) 2147.
[20] G.Y. Kim, S.B. Yi, Y.J. Park, H.G. Kim, Mater. Res. Bull. 43 (2008) 3543.
[21] C.S. Johnson, J.S. Kim, C. Lefief, N. Li, J.T. Vaughey, M.M. Thackeray, Electrochem. Commun. 6 (2004) 1085.
[22] K. Shizuka, T. Kobayashi, K. Okahara, K. Okamoto, S. Kanzaki, R. Kanno, J. Power Sources 146 (2005) 589.
[23] S.H. Kang, M.M. Thackeray, Electrochem. Commun. 11 (2009) 748.